Available online at www.sciencedirect.com
SCIENCE DIRECT®
Energy Conversion and Management 47 (2006) 494–508
ENERGY CONVERSION & MANAGEMENT
www.elsevier.com/locate/enconman

Dissolution mechanisms of CO_2 hydrate droplets in deep seawaters

Jorge Gabitto [a], Costas Tsouris [b,*]

[a] *Prairie View A&M University, Department of Chemical Engineering, P.O. Box 397, Prairie View, TX 77446-0397, USA*
[b] *Oak Ridge National Laboratory, Department of Separations and Materials, P.O. Box 2008, Oak Ridge, TN 37831-6181, USA*

Received 15 November 2004; accepted 27 May 2005
Available online 12 July 2005

Abstract

Carbon dioxide dissolution at intermediate ocean depths was studied using physical and mass transfer models. Particle density and hydrate layer thickness were determined using existing field data. Pseudo-homogeneous and heterogeneous mass transfer models were proposed to study the dissolution process. Pseudo-homogeneous models do not seem to represent the dissolution process well. Although heterogeneous models interpret the physical behavior better, unresolved issues related to hydrate dissolution still remain. For example, solid hydrate forms on one side of the hydrate film while it dissolves on the other. Dissolution is a complex process that comprises at least two sequential steps. The global process is controlled by mass transfer inside the hydrate layer or by a dissolution reaction at the hydrate–water interface.
© 2005 Elsevier Ltd. All rights reserved.

Keywords: CO_2 hydrate; Mass transfer; Ocean carbon sequestration; Hydrate dissolution

* Corresponding author. Tel.: +1 865 241 3246; fax: +1 865 241 4829.
E-mail address: tsourisc@ornl.gov (C. Tsouris).

0196-8904/$ - see front matter © 2005 Elsevier Ltd. All rights reserved.
doi:10.1016/j.enconman.2005.05.016

Nomenclature

A	wetted surface parallel to flow
A_p	mass transfer area
C_D	friction drag coefficient given by Eq. (4)
C_{H_1}	CO_2 concentration on CO_2 side
C_{H_2}	concentration on water side
C_s	CO_2 equilibrium solubility concentration
C_∞	CO_2 concentration in water phase bulk
D	diffusivity
d_p	particle diameter
J_c	molar flow
k_D	dissolution mass transfer coefficient
k_H	mass transfer coefficient through hydrate layer
k_r	formation reaction rate coefficient
k_{rd}	dissolution reaction rate coefficient
k_T	global dissolution rate constant
MW_i	molecular weight of component i
n_p	number of moles
P	pressure
Re	Reynolds number, given by Eq. (6)
s	parameter defined in Eq. (18)
Sc	Schmidt number, given by Eq. (22)
Sh	Sherwood number, given by Eq. (21)
t	time
T	temperature
v	particle velocity

Greek symbols

ε	hydrate layer thickness
μ_i	dynamic viscosity of component i
ν	kinematic viscosity of environmental water
ρ_i	density of component i

Subscripts

H	hydrate
p	particle
w	water

1. Introduction

The disposal of fossil fuel CO_2 in the deep ocean is considered one of the most promising methods to solve the problem of the greenhouse effect [1,2]. Hence, the behavior and stability of liquid CO_2 after it has been delivered into the ocean are very important. At pressures above 4.45 MPa and temperatures below 283.4 K, CO_2 and water form a solid compound known as clathrate, or more commonly CO_2 hydrate [3]. The stability of these solid compounds is a function of the disposal depth, along with other factors such as temperature and salinity [4]. The behavior of the solid hydrate will determine the residence time of the CO_2 injected into the sea. While short residence times will return the CO_2 to the atmosphere, very high rates of dissolution of the solid hydrates into seawater will threaten the marine environment through an unacceptable decrease in the ocean's pH [5].

One of the proposed disposal scenarios is the release of liquid CO_2 at intermediate depths (500–1200 m) using floating platforms [6]. Hydrodynamic instability will induce breakup of the pure CO_2 effluent into liquid droplets. Under the right conditions, these droplets will be covered with a solid hydrate layer. Solid hydrate is known to slow down the dissolution of droplets in seawater [7,8]. Therefore, an understanding of the dissolution process of CO_2 covered droplets is essential for accurate prediction of environmental impact.

Recently, Brewer et al. [9] measured the rates of rise and dissolution of freely released CO_2 droplets in the open ocean. The objective of this research is to study the dissolution process of hydrate covered CO_2 droplets using simple models prepared to interpret the experimental data of Brewer et al. [9].

2. Mechanistic model development

A brief description of the experiments of Brewer et al. [9] is given here. Brewer and his coworkers released a small amount of liquid CO_2 at 800 m open ocean depth and 4.4 °C. The rising droplet stream was imaged using a high definition television camera transported on a remotely operated vehicle. The particles were released inside a simple imaging box, which had a transparent face to the camera and was open to the ocean at the top and bottom. The researchers tracked one particle from a given initial time (t_0). At time t, a second particle appeared in their visual range. They were then able to record the dissolution of the two particles. Their experimental results involved measurements of velocity, particle diameter and physical properties of seawater from depths of 800 m to less than 400 m [9].

In order to interpret their field data, we proposed the following assumptions:

1. Spherical shaped particles have constant particle diameter (d_p).
2. Particles are covered with a uniform hydrate layer of thickness (ε).
3. Particles move at constant terminal velocity (force equilibrium).
4. Particles behave as solid spheres.
5. Particle motion is described by force balance.

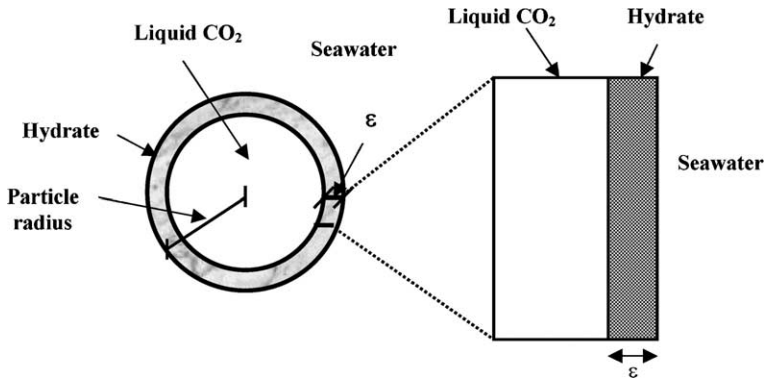

Fig. 1. Ideal CO_2 droplet covered with a hydrate film.

A representation of this ideal particle is shown in Fig. 1. A force balance on a particle similar to the one depicted in Fig. 1 yields

$$\sum \text{forces} = 0 \tag{1}$$

or

$$\text{Drag force} = \text{Buoyancy} - \text{Weight}, \tag{2}$$

where

$$\text{Drag force} = C_D \rho_w v^2 A/2. \tag{3}$$

In Eq. (3), A is the wetted surface parallel to the flow, ρ_w is the seawater density, v is the relative velocity between the particle and the seawater flow and C_D is the friction drag coefficient given by Tek and Wilkes [10]

$$C_D = 18.5/Re^{0.6} \tag{4}$$

$$\text{in the interval } 2 < Re < 2000. \tag{5}$$

Re is the Reynolds number calculated from

$$Re = v d_p \rho/\mu. \tag{6}$$

Here, d_p is the particle diameter and μ is the seawater viscosity.

A combination of Eqs. (2)–(4) yields

$$\rho_p = \rho_w + i(3C_D \rho_w v^2)/(4 d_p g), \tag{7}$$

where i takes the value +1 for a sinking particle and −1 for a floating one.

The hydrate layer thickness (ε) can be calculated from the aforementioned geometrical assumptions as

$$\varepsilon = (\rho_p - \rho_{CO_2}) d_p/(6\rho_H), \tag{8}$$

where ρ_p, ρ_{CO_2} and ρ_H are the hydrate covered particle, liquid CO_2 and solid hydrate densities, respectively. Eq. (8) was derived assuming that

$$r_p \gg \varepsilon \text{ or } d_p + 2\varepsilon \approx d_p. \tag{9}$$

This assumption will be tested once ε is calculated from the experimental data. Combination of Eqs. (2)–(9) allows one to calculate from field measurements of particle size (d_p) and particle velocity (v), the particle density (ρ_p) and hydrate layer thickness (ε) for the particles released in the ocean by Brewer et al. [9].

3. Dissolution model development

In order to understand the CO_2 dissolution process, several models are presented. The procedure followed is the same for all the models: a model is presented, and the equations describing the model are written. Model parameters are calculated using the field and/or physical model calculated data, and a model assessment is performed based upon the calculated values of the parameters.

Starting with a simple pseudo-homogeneous model, we assume that each particle is a homogeneous material whose properties are a combination of liquid CO_2 and solid hydrate properties. A schematic of this model is shown in Fig. 2, including the relevant CO_2 concentrations. Dissolution of the solid material controlled by mass transfer into the seawater leads to

$$\partial n_p/\partial t = -k_D(C_s - C_\infty)A_p \tag{10}$$

or

$$\partial d_p/\partial t = -2k_D \mathrm{MW}_p(C_s - C_\infty)/\rho_p, \tag{11}$$

where n_p is the number of moles of the pseudo-homogeneous material; k_D is a mass transfer dissolution coefficient; C_s is the equilibrium solubility of CO_2 in the environmental water; C_∞ is the CO_2 solubility in the bulk of the environmental water and A_p, MW_p and ρ_p are the external area, molecular weight and density of the particle, respectively.

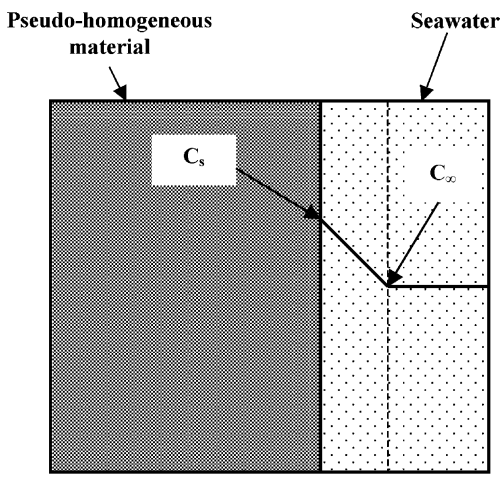

Fig. 2. Representation of the pseudo-homogeneous model.

The second model presented here is a heterogeneous model based upon the work presented by Mori and Mochizuki [8]. The model is represented by a solid hydrate layer (in contact with a liquid CO_2 phase and a liquid seawater phase). The authors propose that CO_2 hydrate is formed on the left side of the hydrate layer (in contact with liquid CO_2), while it is dissolved on the right side (in contact with water). The justification for these assumptions is the finding that the hydrate layer never completely disappears; therefore, simultaneous formation and dissolution processes should be occurring. Because the dissolution process takes place at the water–hydrate interface, the formation process should take place at the other interface. The complexity of hydrate crystal formation and dissolution makes it highly unlikely that simultaneous formation and dissolution occur on the same side [8]. The hydrate layer is assumed to be impermeable to water and/or CO_2 flow at this point. This assumption means that mass flow through the hydrate layer can proceed only by diffusion inside the void space in between the different hydrate crystals. A mass transfer balance yields two equations: one for the liquid CO_2 phase and another for the solid hydrate phase. A schematic depicting the model and the different relevant concentrations is shown in Fig. 3. The mass balance equations are given by

CO_2 phase:

$$\partial n_{CO_2}/\partial t = -k_r C_s A_p \tag{12}$$

or

$$\partial d_p/\partial t = -2k_r \mathrm{MW}_{CO_2} C_s/\rho_{CO_2}. \tag{13}$$

Hydrate phase:

$$\partial n_H/\partial t = [k_r C_s - k_T(C_{H_2} - C_\infty)]A_p \tag{14}$$

or

$$\partial \varepsilon/\partial t + 2\varepsilon/d_p \partial d_p/\partial t = [k_r C_s - k_T(C_{H_2} - C_\infty)]\mathrm{MW}_H/\rho_H, \tag{15}$$

where n_{CO_2} and n_H are the number of moles for the CO_2 and hydrate, respectively; ε is the thickness of the hydrate layer; k_r is the specific reaction rate coefficient for hydrate formation; k_T is the dissolution rate mass transfer coefficient; C_{H_2} is the CO_2 concentration on the right side of the

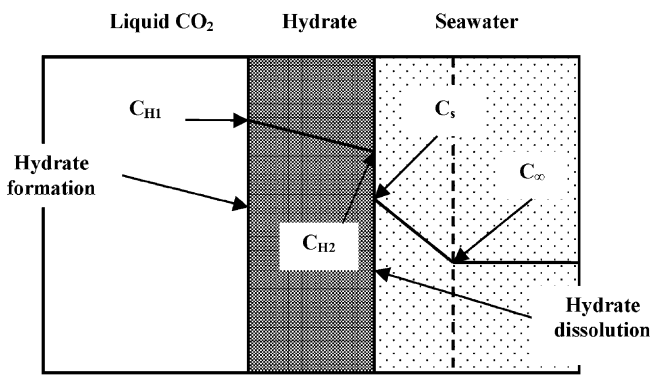

Fig. 3. Representation of heterogeneous model assuming impermeable hydrate layer.

hydrate layer; and MW_H and ρ_H are the molecular weight and density, respectively, of the hydrate layer.

It is an established fact that the hydrate layer forms inside the water side of the liquid CO_2–water interface [11,12]. Therefore, an explanation is needed for the apparent absence of water on the inner side (see Fig. 1) of the hydrate layer. One of the possibilities is intercrystalline-grain water diffusion from the water phase through the hydrate layer. Once the water molecules reach the left side of the hydrate layer, they can be available to react with CO_2 molecules and grow more hydrate. Whether sufficient quantities of water can reach the interface by this mechanism to produce new solid hydrate has yet to be determined.

Mori and Mochizuki [8] proposed that the hydrate layer is not actually impermeable but behaves as a permeable layer. It is assumed that the hydrate film is uniform in thickness and that microperforations are evenly distributed over its full surface. Tortuous capillaries having uniform diameter and length can approximate these microperforations. As a result of the hydrophilic condition of the hydrate phase, capillary forces will fill the capillaries with water. The water that fills the capillaries is saturated with the guest species. Neither formation nor dissociation of the hydrate occurs inside any capillary except for the immediate vicinity of the ends. Fig. 4 depicts a schematic of this model. Mori and Mochizuki [8] find it difficult to support the fact that no hydrate formation/dissolution occurs within the capillaries, and therefore, the capillaries are not "clogged" by the hydrate clusters forming at the CO_2–water interface. In his review of hydrate film formation and metabolic self preservation models, Mori [13] also recognized that the internal texture of polycrystalline hydrate films would be more complex than when they are modeled as regularly perforated plates. Both obstruction of some existing perforations and formation of new ones should occur over the film in order to maintain water flow towards the liquid CO_2 phase. Unfortunately, the Mori and Mochizuki [8] model also introduces several parameters (e.g., tortu-

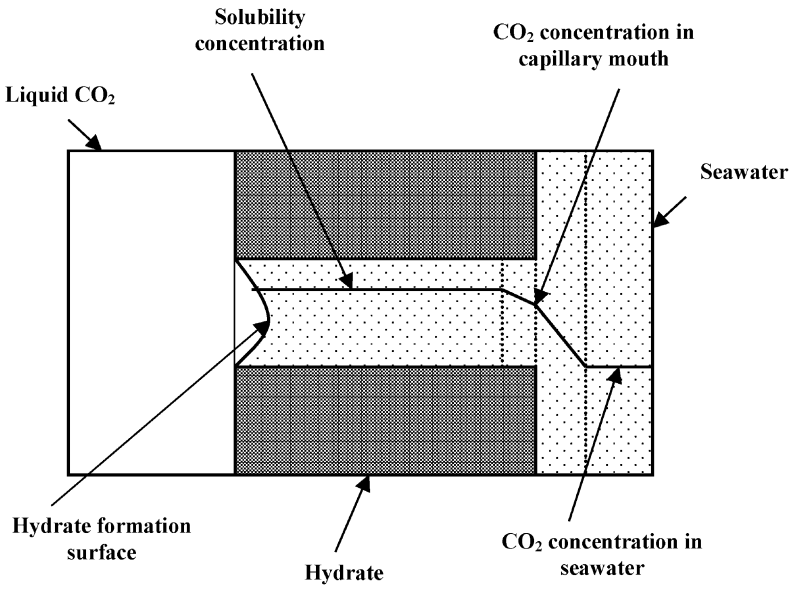

Fig. 4. Schematic of Mori and Mochizuki [8] permeable capillary model.

osity, void fraction, diameter and contact angle between the CO_2 rich phase and the water rich phase) that make quantitative parameter estimation impossible.

Dissolution on the right side of the hydrate layer can proceed by a single layer model in which all the mass transfer resistance is located inside a water side thin film at the hydrate–water interface, or a more complex mass transfer process can be proposed. For example, a two step sequential mass transport mechanism can be proposed: one step involving mass transport through the hydrate layer and the other step involving mass transport across the water thin layer. Ogasawara et al. [14] used this model to describe dissolution of forcibly held droplets subjected to different seawater flow rates. Assuming that this two step model is valid, we have

$$J = k_H(C_{H_1} - C_{H_2})A_p = k_D(C_s - C_\infty)A_p = k_T(C_{H_1} - C_\infty)A_p, \tag{16}$$

where J is the molar CO_2 flow; k_H is a mass transfer coefficient accounting for the resistance through the hydrate layer; and C_{H_1} and C_{H_2} are the CO_2 concentrations in the liquid CO_2–hydrate and hydrate–water interfaces, respectively, calculated from Ogasawara et al. [14].

This process is sequential; therefore, the global mass transfer coefficient can be written as a combination of the individual mass transfer coefficients

$$k_T = sk_Hk_D/(k_H + sk_D). \tag{17}$$

Here, s is a parameter derived from the assumption [14] that a simple relationship exists between the CO_2 concentration inside the hydrate layer and the CO_2 solubility in the water at equilibrium with the hydrate layer, or

$$C_s = C_{H_2}s \tag{18}$$

Eqs. (17) and (18) can be used to estimate k_H.

A variation of this model was proposed by Shindo et al. [15]. In this variation, instead of a mass transport process through the hydrate layer, the authors proposed a dissolution reaction at the hydrate–water interface followed by single layer mass transfer resistance on the water side. Eq. (17) becomes

$$k_T = k_{rd}k_D/(k_{rd} + k_D), \tag{19}$$

where k_{rd} is the dissolution reaction rate constant at the hydrate–water interface.

It is also not clear what values should be used for calculation of C_s. A first approximation is to use liquid CO_2 equilibrium dissolution values that are a function solely of ambient pressure and temperature. Hirai et al. [16] proposed that the real value to be used (C_o) is actually different from the equilibrium solubility of the liquid CO_2. The authors also estimated this value to be approximately one half of the equilibrium solubility. The authors speculated that if the hydrate layer were permeable and crossed by water filled capillaries, the CO_2 concentration inside the capillaries would be different from the concentration in the environmental water in contact with solid hydrate. Mori and Mochizuki [18] concluded that the actual CO_2 solubility in the presence of a hydrate layer is different from that in the absence of a hydrate layer. The authors used experimental data by Kimuro et al. [17] and Aya et al. [18] to show that the value of the CO_2 equilibrium solubility concentration when hydrate is present is different from the equivalent value when hydrate is not present. The authors summarized the nature of the solubility in the hydrate forming region (i.e. temperature lower than the temperature for hydrate formation (T_H)) as follows. The

solubility at a given (P, T) condition has two possible values: the higher value is obtained in the metastable regime in the absence of any hydrate phase in the liquid CO_2–water system, while the lower value is obtained at the same conditions but in the presence of a hydrate phase. The metastable solubility increases as the temperature decreases, while the solubility in the presence of hydrate decreases, thereby expanding the difference between the two sets of values.

The metastable curve is obtained by extrapolating the solubility–temperature relationship in the range $T > T_H$, while the "hydrate-present" curve can be estimated by using the method proposed by Holder and Warzinski [19]. The authors recommended using solubility data in the absence of hydrate [20] combined with the hydrate temperature-forming curve as a function of pressure, $T_H(P)$, to estimate the solubility in the presence of hydrate. In this work, the CO_2 solubility was estimated from the experimental data provided by Aya et al. [18].

Eqs. (17)–(19) can be used to calculate the mass transfer coefficient through the hydrate layer (k_H) from the values of k_T and k_D. Several correlations have been proposed to calculate k_D values. For convenience, the following correlation, taken from Hirai et al. [16], was used in this work

$$Sh = 2 + 0.6Re^{0.5}Sc^{0.333}, \tag{20}$$

where Sh and Sc are dimensionless numbers given by

$$Sh = k_i d_p / D, \tag{21}$$

and

$$Sc = v/D, \tag{22}$$

where k_i is a mass transfer coefficient, D is the diffusivity of CO_2 in the environmental water and v is the kinematic viscosity of the environmental seawater.

4. Results and discussion

Calculations using the field data reported by Brewer et al. [9] are represented in Figs. 5–7. Fig. 5 shows that the particle diameter changes linearly with time. The field data for the two particles

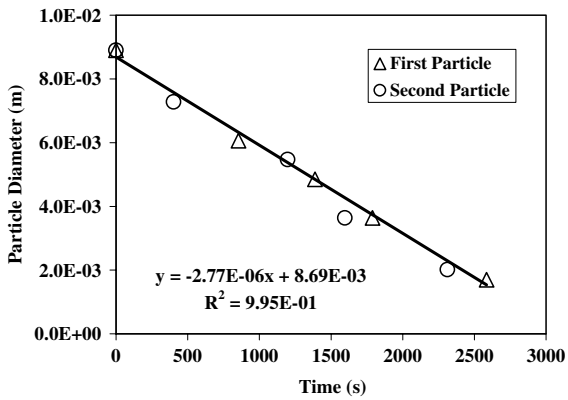

Fig. 5. Variation in particle diameter with time. Data plotted using field data of Brewer et al. [9].

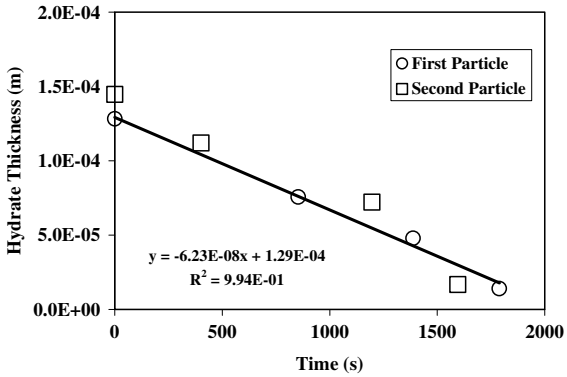

Fig. 6. Hydrate-layer thickness as a function of time for both CO_2 droplets. Data plotted using field data of Brewer et al. [9].

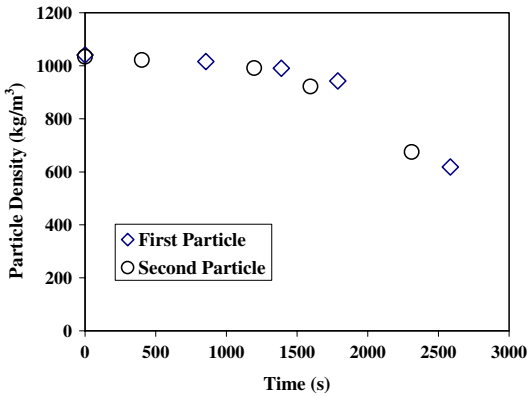

Fig. 7. Variation in particle density with time, plotted using field data of Brewer et al. [9].

reported by Brewer et al. [9] can be correlated using a single straight line. Fig. 5 also suggests that the dissolution behavior of both particles is the same.

Fig. 6 depicts the change in hydrate layer thickness as time increases calculated according to Eq. (8). The hydrate layer thickness decreases linearly with time. The shrinkage of the hydrate layer for both particles can also be represented by a single straight line.

In our calculations, the final field data corresponding to both particles yielded a negative value for hydrate thickness. This finding shows that for very small particles, the model described by Eqs. (2)–(9) is not valid. The proposed model assumes a continuous decrease in the value of the hydrate layer thickness value. Therefore, at sufficiently long periods of time, the hydrate layer should disappear ($\varepsilon = 0$). However, this behavior has not been observed in experiments in which dissolution rate measurements proved that a hydrate layer is always present [8]. Based upon information available in the literature [21], a constant hydrate layer thickness of 10 μm was adopted when our calculated values fell below zero.

Fig. 7 shows the calculated particle density values (ρ_p) for both carbon dioxide particles. The results shown in Figs. 5–7 prove that the dissolution behavior for both particles is very similar. All calculations done during this research project showed essentially no difference in the results calculated for the two particles.

In order to study the dissolution process, we used the measured and/or calculated data presented in Figs. 5–7 to determine the parameters of the different mass transfer models. In the case of the pseudo-homogeneous model, the calculated parameter was the material dissolution coefficient, k_D. Fig. 8 shows the variation of the dissolution coefficient with Reynolds number. Although the dissolution coefficient increases continuously as Reynolds number increases, the rate of increase decreases. Fig. 8 also shows values of the dissolution coefficient for the first particle calculated from Eq. (20). These results show disagreement between the mass transfer coefficients calculated using the pseudo-homogeneous model and Eq. (20). Fig. 9 plots the variation in the dimensionless mass transfer coefficient (*Sh*) vs. Reynolds number. Mass transfer results for the first particle calculated using Eq. (20) are also plotted in the figure. In both cases, the Sherwood number (*Sh*) increases linearly with Reynolds number within the range studied. Although the two sets of results differed by almost an order of magnitude, the slopes are almost the same. The mass transfer coefficients calculated using the model are based on values for liquid CO_2 equilibrium

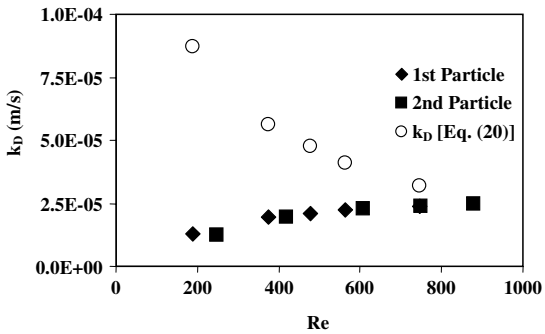

Fig. 8. Mass transfer dissolution coefficient vs. Reynolds number.

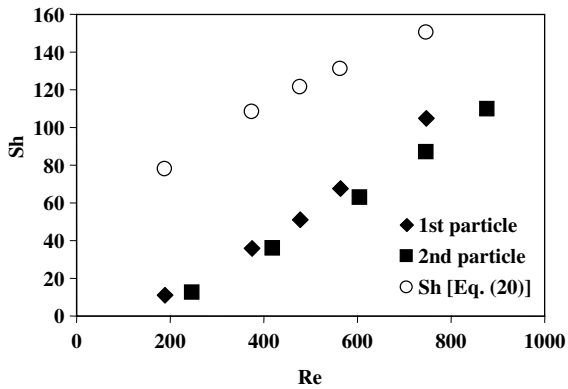

Fig. 9. Dimensionless mass transfer dissolution coefficient vs. Reynolds number.

solubility. Smaller CO_2 concentrations will produce larger mass transfer coefficients in the model, thus decreasing the discrepancy between the two sets of data.

In conclusion, we can say that the pseudo-homogeneous model does not appear to predict correctly the expected variation of the mass transfer coefficient with Reynolds number. Our results also suggest that the use of equilibrium solubility data without hydrate present leads to underestimation of the value of the mass transfer coefficient.

Values of the different parameters corresponding to the heterogeneous model are shown in Fig. 10. The model predicts constant values for the specific reaction rate constant on the left side of the CO_2–hydrate interface. It can be seen that a global dissolution rate coefficient (k_T) decreases slowly as time increases. The model assumes a two step sequential mass transfer process in which the global dissolution rate coefficient (k_T) is given by Eq. (17). The hydrate layer mass transfer coefficient (k_H) was calculated using the global dissolution rate coefficient (k_T) predicted by the model and the water layer mass transfer coefficient (k_D) predicted by Eq. (20). Fig. 10 shows that the global process rate is controlled by the value of the mass transfer coefficient inside the hydrate layer (k_H). Similar results (with even better agreement) were obtained by calculating the dissolution reaction rate coefficient (k_{rd}) proposed by Shindo et al. [15]. Therefore, we can conclude that dissolution is a complex process controlled by mass transport or by a dissolution chemical reaction on the hydrate layer. Similar conclusions were drawn by Shindo et al. [15].

In order to shed light on the nature of the controlling step, we plotted (in Fig. 11) the value of the mass transfer coefficient inside the hydrate layer (k_H) vs. the Reynolds number. Our results indicate that an increase occurs in the value of the mass transfer coefficient inside the hydrate layer (k_H) as the Reynolds number increases. Similar results were reported by Ogasawara et al. [14] in their study of the dissolution of stationary hydrate covered CO_2 droplets. It can be proposed that mass transfer through the hydrate layer is driven by diffusion through grain boundaries in the polycrystalline hydrate. In this case, the value of the mass transfer coefficient inside the hydrate layer (k_H) is given by

$$k_H = D/\varepsilon, \tag{23}$$

where D is the diffusivity of CO_2 in the hydrate layer.

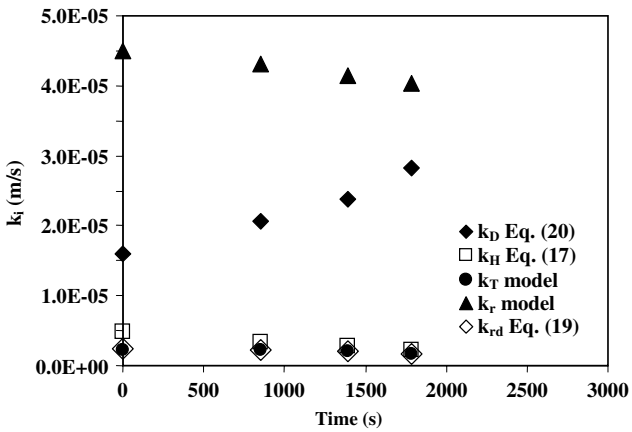

Fig. 10. Heterogeneous model parameter values as a function of time.

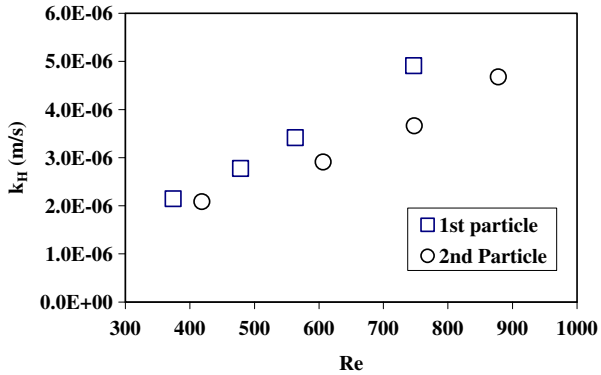

Fig. 11. Hydrate layer mass transfer coefficient vs. Reynolds number.

Eq. (23) can be used to calculate the effective diffusivity through the hydrate layer. Normally, effective diffusivities are approximately constant after the effect of changing layer thickness (ε) has been taken into account [4]. The calculated values plotted in Fig. 12 show a clear dependence of the effective diffusivity on Reynolds number. This finding suggests that an effect exists that is not taken into account in the proposed model. The model assumes that the CO_2 solubility in the environmental water is the equilibrium solubility in the presence of hydrate [8]. Therefore, the solubility at a given temperature and pressure should be independent of the Reynolds number, which is clearly not the case. A possible explanation is that the system does not reach the solubility equilibrium value at the hydrate–water interface. As a result, the actual CO_2 concentration in the environmental water is lower than the equilibrium value and dependent on kinetic effects represented by the Reynolds number. A possible explanation could be mass transfer limitations on the right hand end of the capillaries (see Fig. 4). Unfortunately, we can only speculate about this effect.

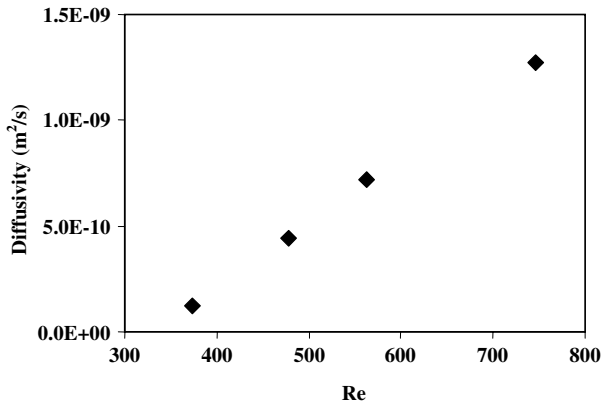

Fig. 12. Hydrate layer effective diffusivity as a function of Reynolds number.

5. Conclusions

A simple mechanistic model predicts the density and hydrate layer thickness values for hydrate covered particles released in the sea. The droplet diameter and hydrate layer thickness decrease linearly with time. The value for the hydrate layer thickness decreases constantly when exposed to unsaturated environmental seawater. Although this simple model predicts ultimate disappearance of the hydrate layer, this prediction is opposed to the experimental information. A correction was suggested to account for the finding that the hydrate film did not disappear.

Pseudo-homogeneous models do not explain well the dissolution process. A heterogeneous model in which solid hydrate is constantly formed on the liquid CO_2–hydrate interface and solid hydrate is dissolved on the hydrate–water side seems to explain more precisely the dissolution behavior of the droplets. Solid hydrate formation at the liquid CO_2–hydrate interface can be explained by assuming either inter-crystalline water diffusion through an impermeable layer or the presence of a permeable hydrate layer. In the permeable model, as a result of the hydrophilic characteristics of the hydrate film, capillary forces filled the capillaries with water. The dissolution of the hydrate layer is a complex process that consists of at least two sequential mass transport steps. The process is controlled either by mass transfer through the hydrate layer or by a dissociation reaction at the hydrate–water interface. The controlling step is not a simple diffusive inter-crystalline process. It is dependent upon the flow condition outside the hydrate layer. This finding suggests the presence of non-equilibrium conditions at the hydrate–water interface.

Acknowledgement

Support by the Nuclear Regulatory Commission, HBCU Minority Education Institutions Faculty Research Participation Program (Jorge Gabitto) and the Ocean Carbon Sequestration Program, Office of Biological and Environmental Research, US Department of Energy, Grant No. KP120203, under contract DE-AC05-00OR22725 with UT-Battelle, LLC, are gratefully acknowledged. We would like to thank Dr. Marsha Savage for editing the manuscript.

References

[1] Reck RA, Hoag KJ. A comparison of greenhouse gas mitigation options. Energy 1997;22(2–3):115–20.
[2] US Department of Energy. Carbon sequestration research and development. Washington, DC: office of Science and Office of Fossil Energy; 1999.
[3] Lee S-Y, Holder GD. AIChE J 2002;48:161–7.
[4] Sloan ED. Clathrate hydrates of natural gases. New York: Marcel-Dekker Inc.; 1998.
[5] Tamburri MN, Peltzer ED, Friederich GE, Aya I, Yamane K, Brewer PG. Marine Chem 2000;72:95–101.
[6] Ozaki M, Sonoda K, Fujioka Y, Tsukamoto O, Komatsu M. Sending CO_2 into deep ocean with a hanging pipe from floating platform. Energy Convers Manage 1995;36(6–9):475–8.
[7] Hirai S, Okazaki K, Tabe Y, Hijikata K, Mori YH. Dissolution rate of liquid CO_2 in pressurized water flows and the effect of clathrate-films. Energy 1997;22(2–3):285–93.
[8] Mori YH, Mochizuki T. Dissolution of liquid CO_2 into water at high pressures: A search for the mechanism of dissolution being retarded through hydrate-film formation. Energy Convers Manage 1998;39(7):567–78.

[9] Brewer PG, Peltzer ET, Friederich G, Rehder G. Experimental determination of the fate of rising CO_2 droplets in seawater. Environ Sci Technol 2002;36:5441–6.
[10] Tek MR, Wilkes JO. Fluid flow and heat transfer. Ann Arbor: University of Michigan; 1974.
[11] Sugaya M, Mori YH. Behavior of clathrate-hydrate formation at the boundary of liquid water and a fluorocarbon in liquid or vapor state. Chem Eng Sci 1996;51(13):3505–17.
[12] Uchida T, Ebinuma T, Kawabata J, Narita H. Microscopic observations of formation processes of clathrate-hydrate films at an interface between water and carbon dioxide. J Cryst Growth 1999;204:348–56.
[13] Mori YH. Clathrate hydrate formation at the interface between liquid CO_2 and water phases—A review of rival models characterizing "hydrate films". Energy Convers Manage 1998;39(15):1537–57.
[14] Ogasawara K, Yamasaki A, Teng H. Mass transfer from CO_2 drops traveling in high-pressure and low-temperature water. Energy Fuels 2001;15:147–50.
[15] Shindo Y, Hakuta T, Fujioka Y, Takeuchi K, Komiyama H. Controlling effect of CO_2 hydrate membrane on CO_2 dissolution into water from the surface of liquid CO_2. Energy Convers Manage 1995;36(6–9):479–84.
[16] Hirai S, Okazaki K, Araki N, Yazawa H, Ito H, Hijikata K. Transport phenomena of liquid CO_2 in pressurized water flow with clathrate hydrate at the interface. Energy Convers Manage 1996;37(6–8):1073–8.
[17] Kimuro H, Yamaguchi F, Ohtsubo K, Yanagi TK. CO_2 clathrate formation and its properties in a simulated deep ocean. Energy Convers Manage 1993;34(9–11):1089–94.
[18] Aya I, Yamane K, Nariai H. Solubility of CO_2 and density of CO_2 hydrate at 30 MPa. Energy 1997;22(2–3): 263–271.
[19] Holder, GD, Warzinski, RP. American Chemical Society, Division of Fuel Chemistry, vol. 41(4), Preprints 1997. p. 1452.
[20] Dodds WS, Stutzman LF, Sollami BJ. Ind Eng Chem, Chem Eng Data Ser 1996;1:92.
[21] Mori YH, Mochizuki T. Mass transport across clathrate hydrate films—A capillary permeation model. Chem Eng Sci 1997;52(20):3613–6.